HOKKAIDO UNIVERSITY

Title	Influence of Bi-Cu microstructure on the photoelectrochemical performance of BiVO4 photoanode for efficient water splitting
Author(s)	Subramanyam, Palyam; Meena, Bhagatram; Suryakala, Duvvuri; Subrahmanyam, Challapalli
Citation	Solar energy materials and solar cells, 232, 111354 https://doi.org/10.1016/j.solmat.2021.111354
Issue Date	2021-10-01
Doc URL	http://hdl.handle.net/2115/90475
Rights	© <2021>. This manuscript version is made available under the CC-BY-NC-ND 4.0 license http://creativecommons.org/licenses/by-nc-nd/4.0/
Rights(URL)	http://creativecommons.org/licenses/by-nc-nd/4.0/
Type	article (author version)
Additional Information	There are other files related to this item in HUSCAP. Check the above URL.
File Information	MS original.pdf

Influence of Bi-Cu Microstructure on the Photoelectrochemical Performance of BiVO₄ Photoanode for Efficient Water Splitting

Palyam Subramanyam,[1*] Bhagatram Meena,[2] Duvvuri Suryakala,[3] Challapalli

Subrahmanyam[2,*]

[1]Research Institute for Electronic Science, Hokkaido University, Sapporo, Hokkaido 001-0020, Japan.

[2]Department of Chemistry, Indian Institute of Technology Hyderabad, Hyderabad, Telangana, 502285,

India

[3]Department of Chemistry, GITAM University, Visakhapatnam, Andhra Pradesh, 530045, India.

[*]Corresponding author:

Palyam Subramanyam, Email address: subbu@es.hokudai.ac.jp

Challapalli Subrahmanyam, Tel: +91-40-23016050, Email address: csubbu@iith.ac.in

Abstract

To date, photoanodes containing bimetallic alloy nanoparticles (ANPs) are exposed good photoelectrochemical (PEC) performance for hydrogen production owing to their optoelectronic properties. In this work, low-cost, visible light active and environmental-friendly BiVO₄/Bi-Cu nanocomposite photoanode is fabricated via organic decomposition and electrodeposition process. Transmission electron microscope images reveals that Bi-Cu ANPs are uniformly distributed on BiVO₄ which can enhance the PEC performance. Typical results originate that BiVO₄/Bi-Cu nanocomposite exhibits a high photocurrent density of 10.31 mA cm^{-2} at 1.23 V and solar-to-hydrogen conversion efficiency of 3.55%, which is higher than other electrodes. In addition, this composite shows excellent long-term stability over 5 h and low charge transfer resistance. These results suggest the

1

introduction of Bi-Cu ANPs enhances the broadband light absorption of BiVO$_4$ due to the excitation of localized surface plasmons at different wavelengths and also improves the charge transportation in the photoanode. Thus, BiVO$_4$/Bi-Cu photoelectrode reports here is superior PEC performance for hydrogen generation providing an economical and feasible route to fabricate surface plasmon resonance (SPR)-enhanced composites as photocatalysts using earth-abundant Bi and Cu metals instead of noble-metals.

Keywords: Photoelectrochemical cell; BiVO$_4$; Bi-Cu alloy; surface plasmon resonance; charge separation; water splitting

Introduction

Photoelectrochemical (PEC) water splitting for hydrogen production can be done via designing photoelectrodes with high light absorption, quick charge carrier generation and transportation [1-3]. In recent decades, monoclinic bismuth vanadate (BiVO$_4$) has been reported as an efficient photoanode for its advantages like narrow bandgap (2.4 eV), high optical absorption coefficient (10^4-10^5 cm^{-1}) and good photo-stability [4-6]. Moreover, attaining flat band potential (<200 mV) positive to hydrogen evolution reaction (HER) [7] also permits the oxygen evolution reaction (OER) at a lower onset potential than other metal oxides [8, 9]. In addition, BiVO$_4$ also exhibits high theoretical photocurrent density of ~7.5 mA cm^{-2} at 1.23 V *vs* reversible hydrogen electrode (RHE) at 1.5 AM light illumination [5, 7-9]. However, pure BiVO$_4$ photoanode often suffer from low solar to hydrogen (STH) conversion efficiency due to poor transport and low mobility of charge carriers which lead to high recombination of photogenerated electrons. To overcome these issues, various strategies such as doping [10, 11], hetero-nanostructure formation using semiconductors [12] or plasmonic metals [13, 14] and co-catalyst loading [15] have been adopted to enhance the water splitting performance of BiVO$_4$.

Amongst all, the hetero-nanostructure construction with plasmonic metal nanoparticles (such as Au, Ag, Cu, Pd, Pt and Bi) exhibits enhanced light harvesting, improved charge separation and transportation, thus resulting in the improvement of STH efficiency [13,16-20]. Recently, non-noble bismuth metal nanoparticles (Bi NPs) supported $BiVO_4$ photoelectrodes demonstrates unique benefits over noble metals (Au, Ag and Pt) for PEC water splitting [18, 19]. Due to the surface plasmon resonance (SPR) effect of Bi NPs, the optical absorption window expands from UV to IR region and suppresses the rate of carrier recombination in conventional semiconductors [21]. The plasmonic properties of these earth-abundant NPs are yet to be attracted for PEC applications. For example, Wulan et al. reported Bi-$BiVO_4$ photoelectrode with a photocurrent density of 1.96 mA cm^{-2} at 1.23 V *vs* RHE, which is twice that of pristine $BiVO_4$ [22]. Previously, we reported Bi-rGO/$BiVO_4$ photoanode with a photocurrent density of 6.05 mA cm^{-2} at 1.23 V, which is three times higher than pristine $BiVO_4$ electrode [23]. On the other hand, Cu has been widely used in PEC water splitting owing to its low cost, high electronic conductivity and superior photocatalytic activity [24-26]. Moreover, Cu nanoparticles also exhibits SPR effect on contact with conventional semiconductors [27-29]. Recently, Zhang et al., reported Cu/TiO_2 nanotube arrays (TNAs) photoanode showed high PEC performance and good photo-stability for HER under visible light than the pure TNAs due to the SPR of Cu NPs [30]. Li et al., fabricated Cu/ZnO photoanode for PEC water splitting and achieved a high photocurrent density than bare ZnO electrode. This photocurrent enhancement is mainly attributed to the improved electrons conductivity based on the SPR effect of Cu NPs [31].

Recently, bimetallic alloy nanoparticles (ANPs) such as Au-Ag [32], Au-Pd [33, 34], Au-Cu [35], Bi-Ag [36] and Au-Pt [37] have gained great attention for PEC applications due to their unique optoelectronic properties and high stability during the reaction over pure metals. For instance, in Au-Pd alloy, Au NPs acts as good photosensitizer due to SPR, while Pd NPs offer high electrocatalytic activity [38]. Therefore, based on the available reports on

ANPs in PEC water splitting, we were encouraged to examine Bi-Cu due to their unique optical and electronic properties owing to synergic effects between Bi and Cu. To the best of our knowledge, there is no report of Bi-Cu ANPs decorated $BiVO_4$ for PEC water splitting.

In this work, we have decorated $BiVO_4$ film with Bi-Cu ANPs fabricated by drop casting via organic decomposition method followed by electrodeposition. The resultant film is tested for PEC water splitting as a photoanode. A systematic study was performed to understand the influence of Bi-Cu ANPs in the semiconductor photoanode for improving the PEC performance. Finally, a suitable mechanism for the improvement in PEC performance is discussed.

Experimental

Fabrication of $BiVO_4$ photoanode

The $BiVO_4$ photoanode is fabricated as follows: 173 mg of bismuth nitrate pentahydrate was taken in 0.4 ml of glacial acetic acid followed by sonication for 2 min to obtain a clear solution A. On the other hand, vanadyl acetylacetonate (95 mg) was dissolved in acetylacetone (4.6 ml) and sonicated to form a solution B. Now solution A was mixed with solution B and then sonicated for 10 min, a green solution of $BiVO_4$ was obtained. Further, 0.6 ml of $BiVO_4$ solution was drop-casted on conductive substrate (FTO) followed by annealing at 500 °C for 30 min, to form a yellow color film of $BiVO_4$ [23, 39-41].

Fabrication of $BiVO_4$/Bi-Cu/photoanode

$BiVO_4$/Bi-Cu photoanode was prepared using an electrodeposition method. Typically, an electrodeposition process is done using three electrode system, where FTO/$BiVO_4$ is used as working electrode, Pt rod and Ag/AgCl as the counter and reference electrode respectively, while 0.1 M of copper nitrate and 0.1 M of bismuth nitrate in dilute nitric acid solution served as the electrolyte for Bi-Cu deposition. The deposition was carried at -0.5 V for 500 s to obtain dark brownish $BiVO_4$/Bi-Cu electrode. The deposition scheme of $BiVO_4$/Bi-Cu

photoanode as presented in Scheme 1. Similarly, BiVO₄/Bi and BiVO₄/Cu were prepared using pure bismuth nitrate and copper nitrate respectively. Bi NPs, Cu NPs, and Bi-Cu ANPs were also synthesized by the same procedure (electrodeposition method) used to fabricate BiVO4/Bi-Cu. Furthermore, Bi NPs, Cu NPs and Bi-Cu ANPs were scraped off from the FTO substrate and dispersed in ethanol solution for following studies.
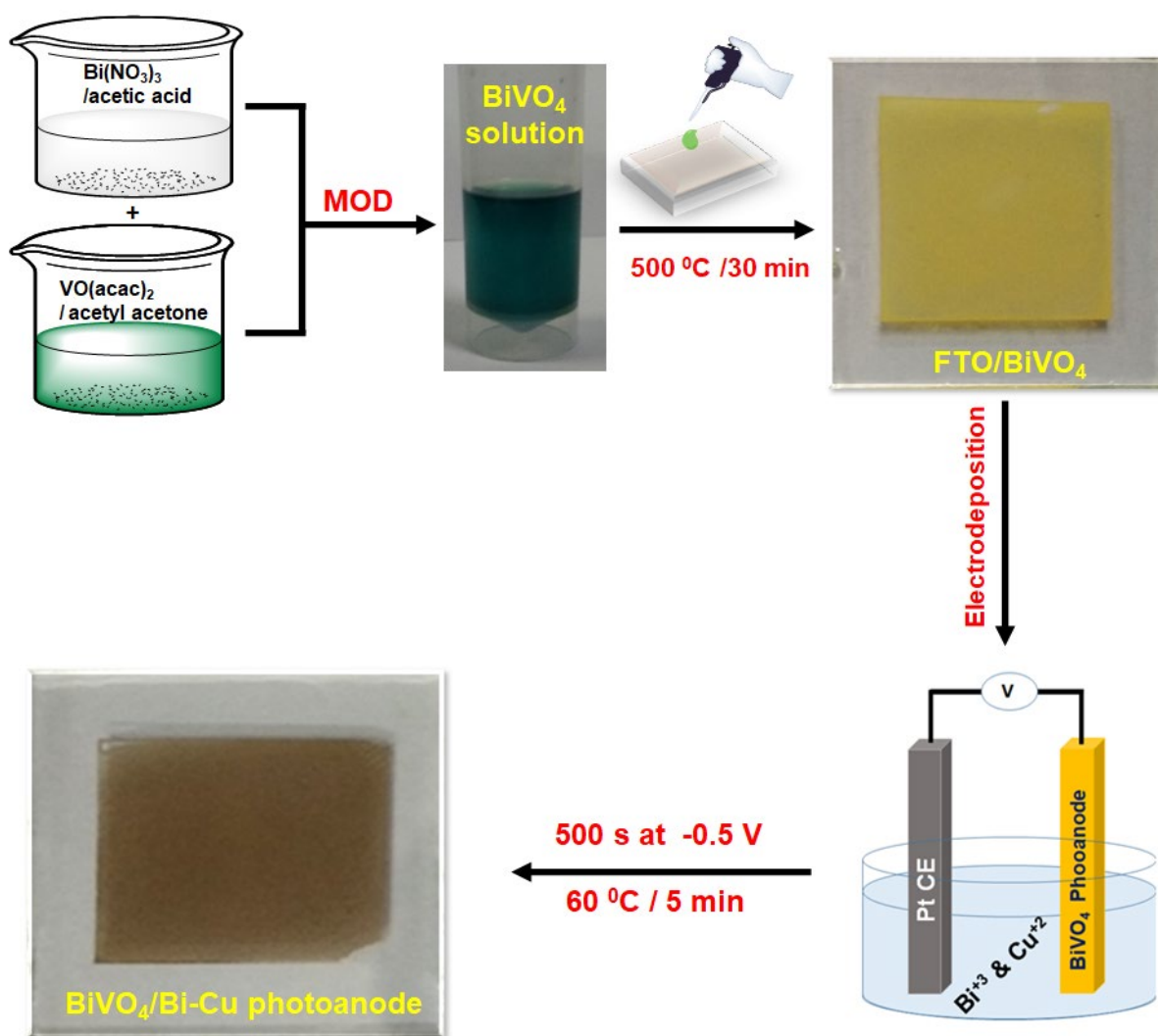

Scheme 1 The deposition scheme of BiVO₄/Bi-Cu photoanode.

Results and discussion

To investigate the optical behavior of the photoactive materials were carried out by UV-visible diffuse reflectance spectrometry and results were shown in Fig. 1a and Fig. 1b. For absorption studies, Bi NPs, Cu NPs and Bi-Cu ANPs were scraped off from the FTO substrate and dispersed in ethanol solution (Fig. 1a). The Fig. 1a reveals that Bi NPs display a sharp surface plasmon resonance peak centered at 320 nm which is extended to near IR [23, 42], while, Cu NPs show a characteristic SPR absorption peak centered at 580 nm [27,28]. For Bi-Cu ANPs, one broad SPR absorption band is observed in the visible to near IR region (400-800 nm) due to the synergistic effect of Bi and Cu (Fig. 1a). BiVO$_4$ clearly reveals a narrow spectral range with an absorption edge at 515 nm, having a bandgap of 2.4 eV (Fig. 1b). Further, BiVO$_4$/Bi NPs show broad absorption range in 300-800 nm region while BiVO$_4$/Cu NPs display broad absorption range in 300-600 nm due to the presence of SPR Bi and Cu, respectively (Fig. 1b). On modification of BiVO$_4$ electrode using Bi-Cu ANPs, the absorption band of the electrode extends from the visible to NIR region and also improves the absorption intensity over other electrodes as shown in Fig. 1b. Furthermore, to determine the light harvesting efficiency (LHE) of the photoactive materials and is expressed by the following equation: LHE = $1-10^{-A}$, where A is the absorbance at wavelength [43, 44] and results were presented in Fig. 1c. Impressively, BiVO$_4$/Bi-Cu ANPs show a high LHE than the others, which is consistent with the observations from absorption spectrum. These results indicate that the improvement of light absorption is favorable to capture more photons and thus generate more excitons, which is supportive for high-generated current density for PEC water splitting. The XRD patterns of BiVO$_4$, Bi NPs, Cu NPs and Bi-Cu ANPs as shown in Fig. 1d, which demonstrate the monoclinic crystal lattice of BiVO$_4$, rhombohedral structure of Bi NPs and face centered cubic lattice of Cu NPs. The XRD patterns of Bi-Cu ANPs exhibits both Bi and Cu peaks, (012), (104), (110), (202), (024) and (112) planes which

corresponds to rhombohedral structure of Bi NPs and three additional peaks at (111), (200) and (220) planes which relates to face centered cubic lattice of Cu NPs. This result confirmed that Bi-Cu ANPs were successfully formed. The detailed analysis of the XRD patterns of $BiVO_4$, Bi NPs and Cu NPs is provided in supporting information.
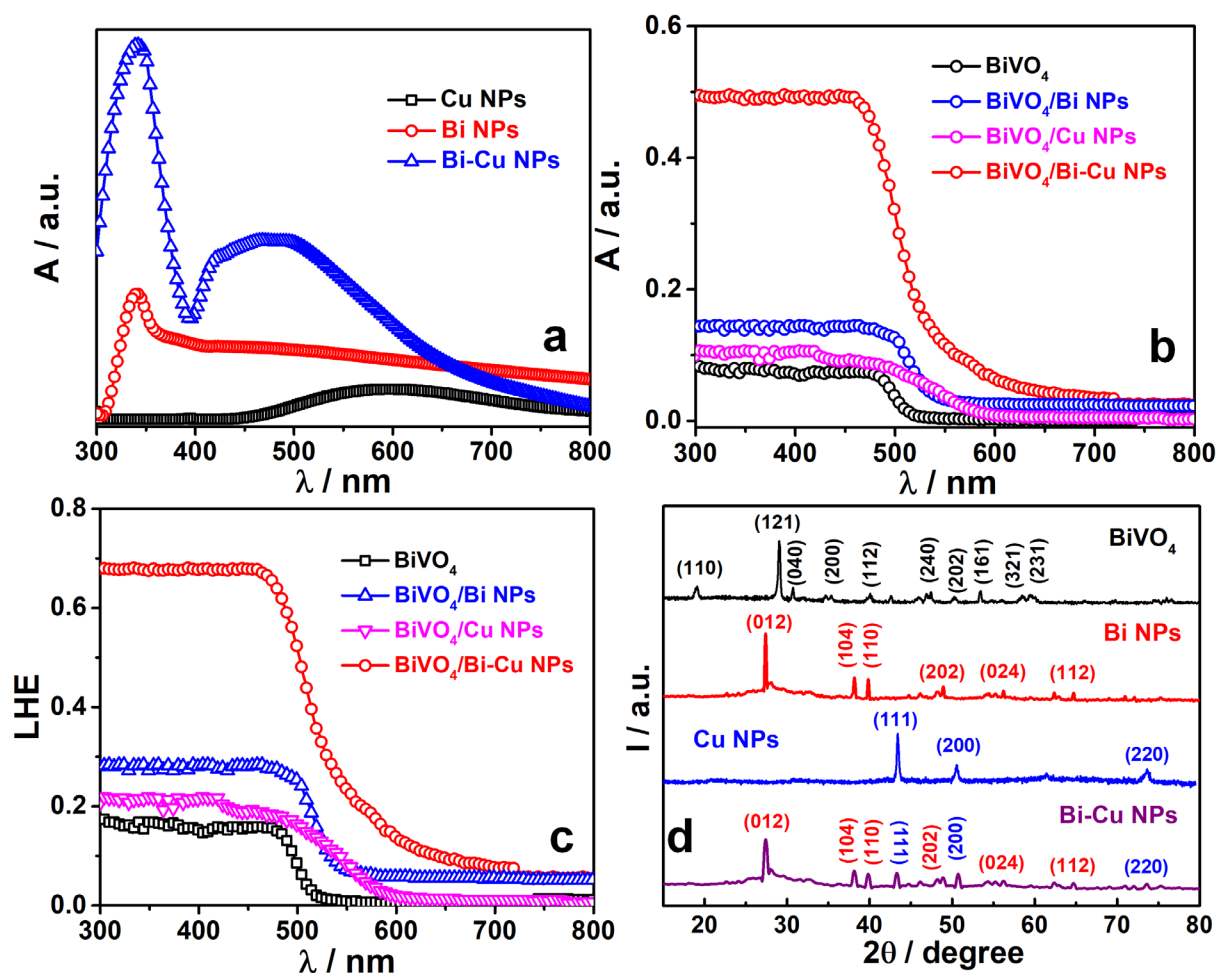
**Fig. 1** Absorption spectra of (a) Bi NPs, Cu NPs and Bi-Cu NPs (b) $BiVO_4$, $BiVO_4$/Bi NPs, $BiVO_4$/Cu NPs and $BiVO_4$/Bi-Cu NPs (c) light harvesting efficacy of $BiVO_4$, $BiVO_4$/Bi NPs, $BiVO_4$/Cu NPs and $BiVO_4$/Bi-Cu NPs and (d) XRD patterns of $BiVO_4$, Bi NPs, Cu NPs and Bi-Cu NPs.

To further conclude the existence of Bi-Cu NPs on $BiVO_4$ semiconductor, the X-ray photoelectron spectroscopy (XPS) was used. The resultant plots for intensity vs binding energy (BE) are shown in Fig. 2. The deconvoluted high-resolution XPS spectra of Bi 4f in

Fig. 2a, two pairs of spin-orbit doublets can be observed in Bi-Cu/BiVO$_4$, suggesting the existence of metal Bi (Bi-Bi bonding energy peaks appeared at 156.7and 161.9 eV) and Bi^{3+} (Bi-O bonding energy peaks at 158.9 and 164.2 eV) [22]. Fig. 2b depicts the XPS spectra of V 2p with the featured binding energies of 516.4 eV and 524.1 eV corresponding to V 2p3/2 and V 2p1/2 respectively [22]. The asymmetric profile of O 1s can be fitted into two symmetrical peaks at 529.6 and 531.8 eV (Fig. 2c), indicating lattice oxygen in BiVO$_4$ and chemisorbed oxygen (OH) by the surface, respectively. Finally, Fig. 2d reveals the XPS of Cu 2p with the featured binding energy position of Cu 2p3/2 at 933.4 eV suggesting existence of Cu NPs [45]. In all XPS spectra, no obvious separate satellite peaks were observed, indicating that the surface of Au-Cu ANPs is effective in protecting Bi and Cu from oxidation. Therefore, the presence of Bi 4f5/2, Bi 4f7/2, O 1S, V 2p3/2, V 2p1/2 and Cu 2p3/2 spin states confirms the existence of Bi-Cu ANPs in the nanocomposite photoanode. In addition, we measured XPS of BiVO$_4$, Bi/BiVO$_4$ and Cu/BiVO$_4$ as shown in Fig. S1. As shown in Fig. S1a and S1b, the binding energies of metallic Bi and Cu are slightly shifted in Bi-Cu/BiVO$_4$ compared to monometallic Bi-BiVO$_4$ and Cu-BiVO$_4$ films, which implies that alloying of Bi-Cu. During alloy particle formation, Bi and Cu adjust their respective Fermi energy levels to the same value through a charge equilibration process, which results in a change in the binding energy value. This positive/negative shift for Bi(4f)/Cu(2p) in the Bi-Cu alloy nanoparticles is known to be evidence of their strong tendency to lose electrons and high catalytic properties. On the other hand, the binding energy of Bi^{3+} species (Bi 4f) in BiVO$_4$ was located at 159.1 eV and 164.4 eV as shown in Fig. S1a, similar to the previous literature [46-48]. The peak of Bi^{3+} is negatively shifted in Bi/BiVO$_4$ and Bi-Cu/BiVO$_4$ as compared to that of pristine BiVO$_4$ (Fig. S1a). Indeed, this observation completely proves that there is a Fermi level equilibrium between metals or bimetals and BiVO$_4$, which promotes effective electron transfer between the Bi-Cu alloy and the conduction band of BiVO$_4$.
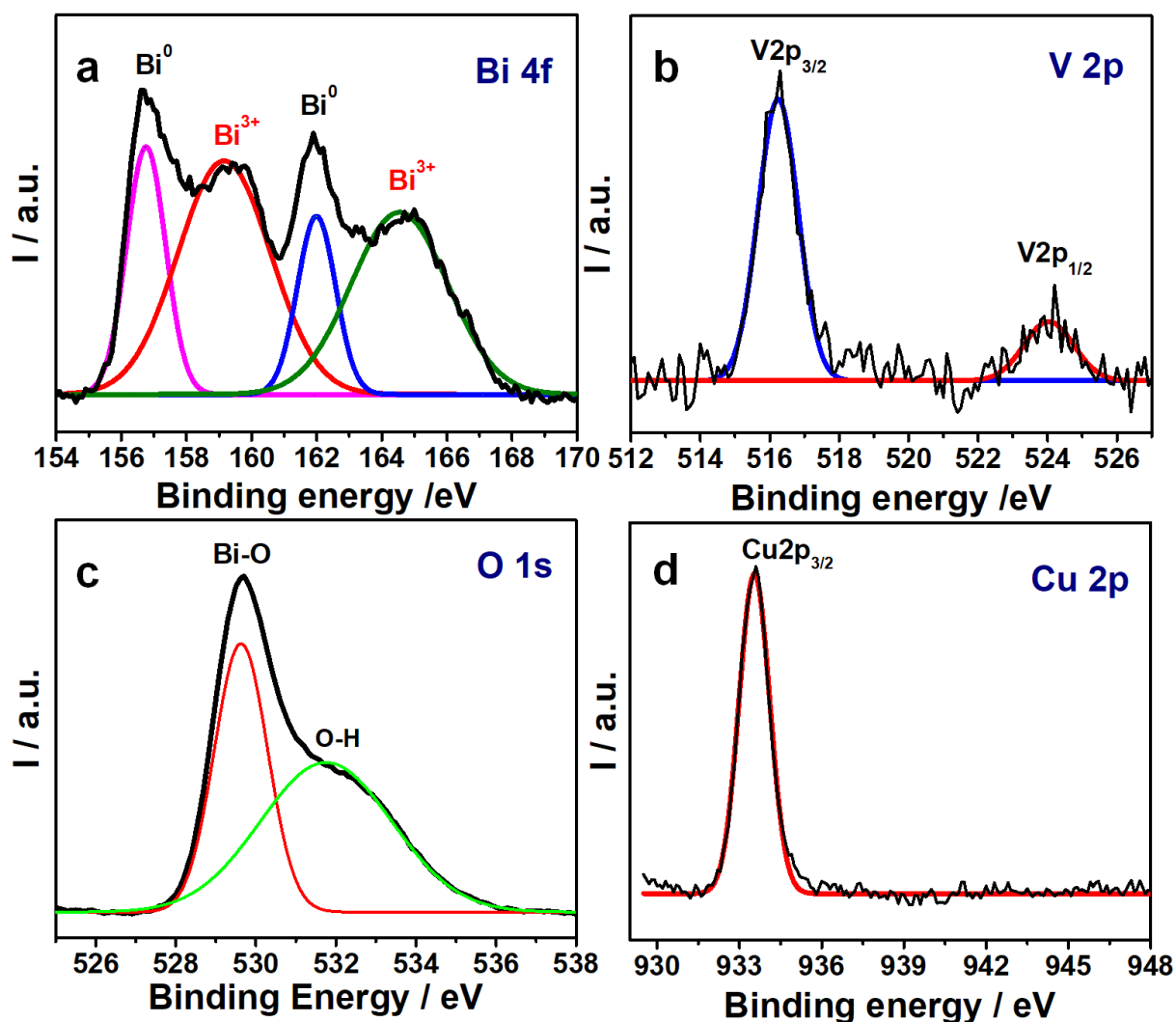
Fig. 2 High-resolution XPS region spectra of (a) Bi 4f, (b) V 2p, (c) O 1s and (d) Cu 2p for the $BiVO_4$/Bi-Cu nanocomposite.

Further, FE-SEM analysis was used to study the morphology of the samples such as $BiVO_4$ and $BiVO_4$/Bi-Cu composite and results were displayed in Fig. 3. The surface morphology of $BiVO_4$ appears to be porous irregular flake like structure with an average diameter of 320-340 nm as shown in Fig. 3a. Fig. 3b displays the presence of Bi-Cu ANPs on $BiVO_4$ which are aggregated and randomly dispersed with no specific shape and high roughness. The surface morphology of Bi-Cu ANPs reveals spherical shape morphology with an average diameter of 30-50 nm (Fig. S2a). Further, elemental mapping analysis and electron diffraction X-ray (EDAX) images confirm the formation of the Bi-Cu ANPs, which

9

are shown in Fig. S2b and S2c, respectively. Further, HRTEM image of BiVO$_4$/Bi-Cu sample reveals the placement of Bi-Cu alloys on BiVO$_4$ (Fig. 3c, 3d and 3e) and the lattice fringes of individual components (Fig. 3f). Monoclinic structure of BiVO$_4$ has the lattice spacing of 0.31 nm that corresponds to (121) (JCPDS-140688). Plasmonic Bi NPs has the lattice spacing of 0.23 nm which is assigned to (110) plane (JCPDS-851331), while face centered cubic Cu NPs have the lattice spacing of 0.21 nm that is assigned to (111) plane (JCPDS-892838). The TEM image of Bi-Cu ANPs and BiVO$_4$ are shown in the supporting information. Bi-Cu ANPs show spherical morphology with particle diameter is around 20-30 nm (Fig. S2d). Further, HRTEM with lattice fringes (Fig. S2e) and selected area electron diffraction (SAED) patterns (Fig. S2f) confirm the formation of the Bi-Cu ANPs. From Fig. S3, BiVO$_4$ reveals irregular spherical shape with particle diameter is approximately 100 nm.
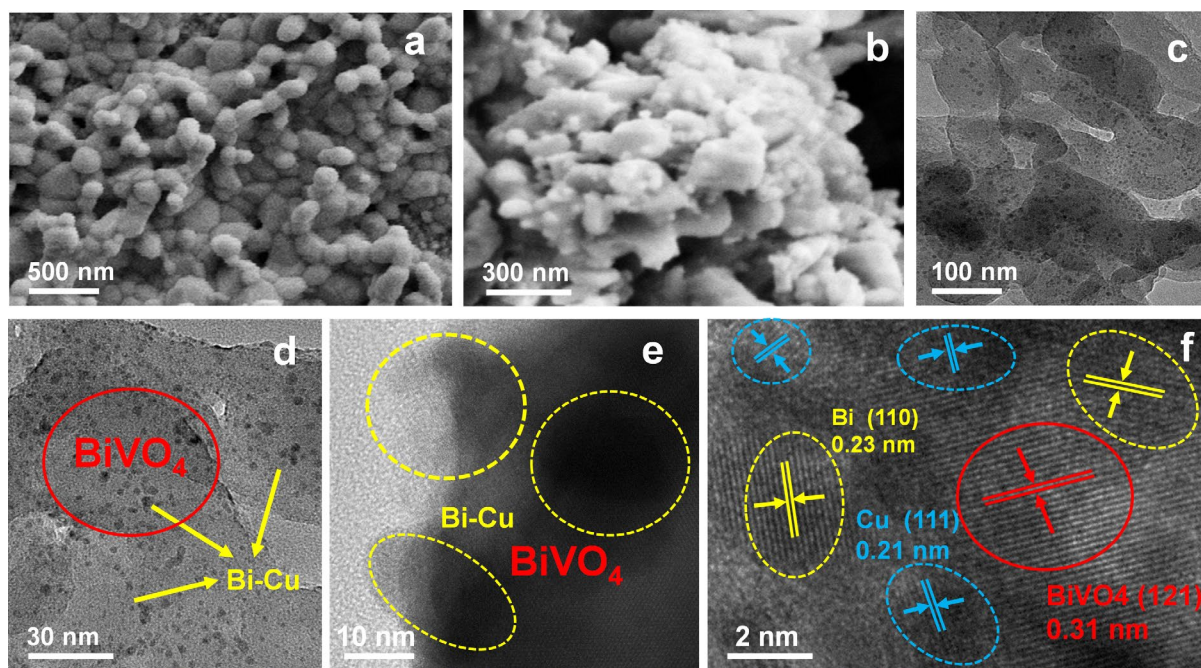

Fig. 3 FE-SEM images of (a) BiVO$_4$ and (b) BiVO$_4$/Bi-Cu and HRTEM images of (c)-(e) BiVO$_4$/Bi-Cu (f) lattice fringes of BiVO$_4$/Bi-Cu composite.

The PEC activity of as-fabricated photoanodes was evaluated for water splitting by LSV plots in three-electrode system (Ag/AgCl as the reference electrode and Pt as the

counter electrode). LSV experiments were recorded in the range of -0.6 V to 0.8 V vs. Ag/AgCl with a scan rate of 50 mV s^{-1} and the results are summarized in Fig. 4a. The pH of the electrolyte was set at 7 and all the potentials are reported versus RHE that are calculated using Nernst equation (SI). All electrodes have an active area of 1 cm^2. Upon chopped light illumination, BiVO$_4$, BiVO$_4$/Cu NPs, BiVO$_4$/Bi NPs and BiVO$_4$/Bi-Cu composites showed photocurrent density of 2.91, 3.55, 5.63 and 10.31 mA cm^{-2} at 1.23 V, respectively (Fig. 4a). The highest photo-response in terms of current density is observed for BiVO$_4$/Bi-Cu at the lowest onset potential of 0.22 V. The enhanced photocurrent density of BiVO$_4$/Bi-Cu electrode, which is promising for PEC water splitting, is attributed to the synergetic effects of BiVO$_4$ and Bi-Cu ANPs. The enhancement is due the light sensitization ability of BiVO$_4$ and Bi-Cu ANPs exhibiting SPR effect with high conductivity. In addition, the efficiency of a photoelectrode is expressed in terms of STH conversion. The STH conversion efficiencies for BiVO$_4$, BiVO$_4$/Cu NPs, BiVO$_4$/Bi NPs and BiVO$_4$/Bi-Cu are estimated to be 1.08, 1.36, 1.81 and 3.55 % at 0.68 V (Fig. 4b), which are calculated from short circuit current density and intensity of incident light (SI). BiVO$_4$/Bi-Cu photoanode provides us with 2-fold and 3-fold higher STH conversion efficiency than BiVO$_4$/Bi NPs and BiVO$_4$/Cu NPs respectively. This indicates the presence of Bi-Cu ANPs enhanced the light harvesting as well as electrons conductivity and charge carrier separation of BiVO$_4$. Further, the stability of photocurrent response by BiVO$_4$, BiVO$_4$/Cu NPs, BiVO$_4$/Bi NPs and BiVO$_4$/Bi-Cu photoanodes is examined by chronoamperometric (I-t curve) studies. Also, the photocurrent responses of the electrodes are tested at 1.23 V *vs* RHE under light irradiation, and the results are presented in Fig. 4c. The long-term stability of the BiVO$_4$/Bi-Cu photoanode is noteworthy; no decay in performance is observed after 5 h. In addition to the stability measurements, the evolved gases during the continuous chronoamperometry tests were analyzed by gas chromatography. In these experiments, the device structure was conducted in a sealed quartz reactor in a gas-tight environment and evolved gases were collected using an airtight syringe. H$_2$ evolved

is plotted as a function of time at 1.23 V vs RHE. As shown in Fig. 4d, the BiVO$_4$/Bi-Cu photoanode provides maximum H$_2$ evolution (1251 μmol) over 2 h compared to pristine BiVO$_4$ photoanode (544 μmol). The high photocurrent and H$_2$ evolution performances of BiVO$_4$/Bi-Cu photoanode are in good agreement.
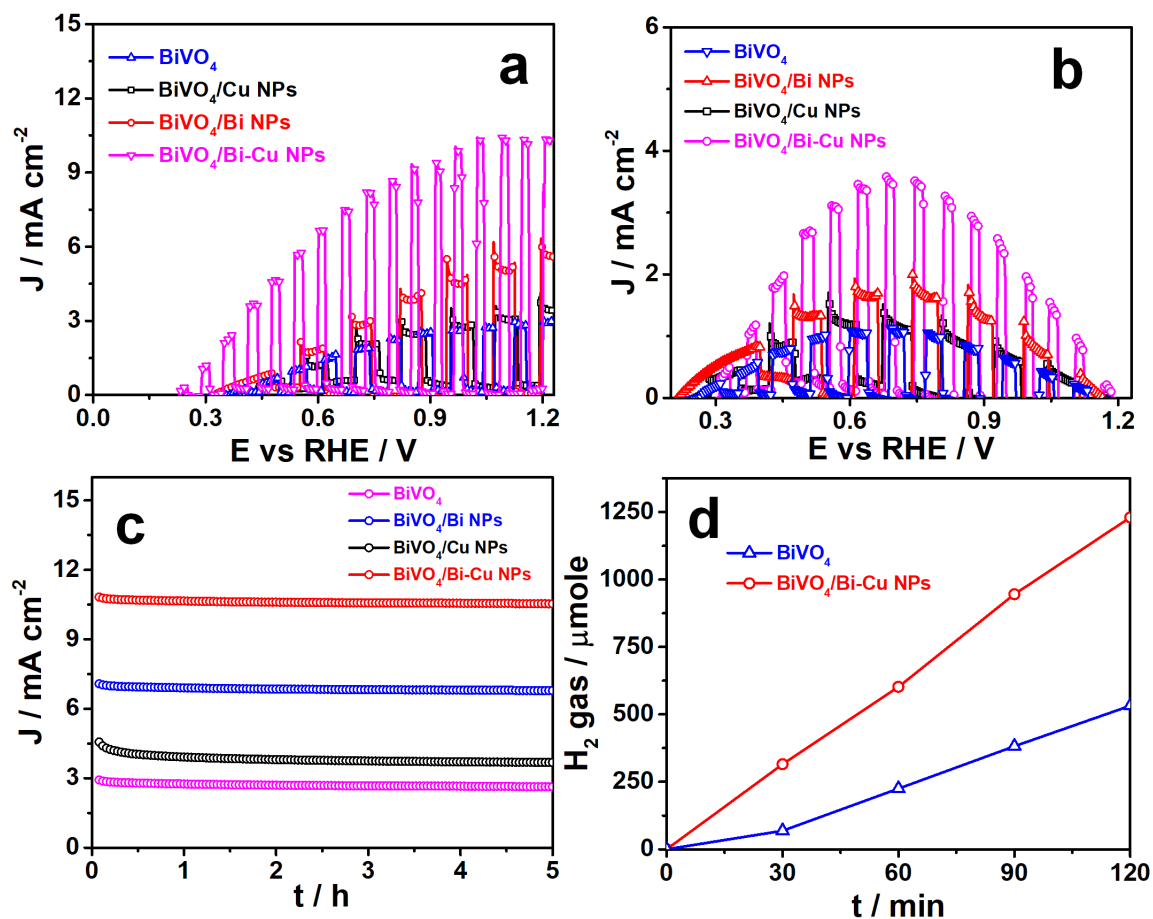
Fig. 4 (a) LSV plots, (b) STH efficiency, (c) photocurrent stability plots of BiVO$_4$, BiVO$_4$/Cu NPs, BiVO$_4$/Bi NPs and BiVO$_4$/Bi-Cu photoanodes and (d) Temporal evolution of H$_2$ gas by BiVO$_4$ and BiVO$_4$/Bi-Cu electrodes.

The ability of photoelectrodes to convert the incident photons into electrons is examined by IPCE experiments using a two-electrode system, but without any external bias and results are shown in Fig. 5a. The maximum IPCE for BiVO$_4$ is 25% in the visible region from 400-515 nm. There's an increase in IPCE for BiVO$_4$ electrode supplemented with Bi NPs, which is 34% in 400-515 nm region and additional contribution of 2-10% in the

515-800 nm region. This enhancement in IPCE performance by Bi NPs is attributed to their SPR effects in the visible to NIR region. When compared to the 25% IPCE of $BiVO_4$ alone, $BiVO_4$/Cu NPs electrode shows ca 29 IPCE in the 400-515 nm region, which is contributed by high electrical conductivity and SPR effect of Cu NPs. Thus, by combining the plasmonic effect with high electrical conductivity of Bi-Cu NPs, in $BiVO_4$/Bi-Cu we accomplish 42% IPCE in the 400-515 nm and additional contribution of 8-15% in the 515-800 nm region. Also, this result implies that Bi-Cu ANPs in the $BiVO_4$/Bi-Cu suppresses undesired recombination of photogenerated charge carriers in $BiVO_4$. Further, the kinetics of charge injection at the photoanode/electrolyte interface is studied by measuring the resistance across electrode/electrolyte interface. Here, impedance measurements were carried out under the light illumination of $BiVO_4$, $BiVO_4$/Cu NPs, $BiVO_4$/Bi NPs and $BiVO_4$/Bi-Cu electrodes immersed in a solution of 0.1 M Na_2SO_4 and the plots were fitted into the equivalent circuits shown in inset Fig. 5b, where R_S, R_{CT} and CPE represent the electrolyte solution resistance, interfacial charge transfer resistance at the electrode/electrolyte and constant phase element for photoelectrode/electrolyte, respectively. The fitted parameters are given in Table 1 (SI). All the electrodes have solution resistance (R_S) lie in the range of 8-9 Ω. The high R_{CT} value of 196 Ω for $BiVO_4$ is due to low charge separation and lowest R_{CT} value of 21 Ω for $BiVO_4$/Bi-Cu photoanode compared to other electrodes, indicating the facile transfer of charge carriers at the $BiVO_4$/Bi-Cu photoanode/electrolyte interface, which is consistent with the excellent PEC performance of the electrode. Also, this charge injection property is consistent with the electron lifetime (τ) values estimated from Bode plots (Fig. S4). The τ values are estimated using the relation: $\tau = 1/(2\pi f_{max})$ where f_{max} is the frequency maxima. The τ values calculated for pristine $BiVO_4$, $BiVO_4$/Cu NPs, $BiVO_4$/Bi NPs and $BiVO_4$/Bi-Cu films are 2.41, 8.75, 11.53 and 13.86 ms, respectively. The large τ value corresponds to high rate of carrier transport or low rate of undesired carrier recombination in $BiVO_4$/Bi-Cu photoelectrode, which is attributed to the effect of Bi-Cu ANPs due to the formation of

Schottky barrier at the interface between Bi-Cu alloy and BiVO$_4$ also helps the transferred hot electrons accumulate in the BiVO$_4$, preventing them from traveling back to the Bi-Cu ANPs. In other words, Bi-Cu ANPs increases the τ value of BiVO$_4$/Bi-Cu, which is in good agreement with the higher photocurrent density. Furthermore, the Mott-Schottky plots of electrodes (Fig. S5a) were plotted, where the linear profiles with positive slope confirmed that the photoelectrodes are n-type. On extrapolation of intercept on the x-axis, flat band potential (V$_{FB}$) was estimated which are found to be 0.42, 0.37, 0.35 and 0.31 V for BiVO$_4$, BiVO$_4$/Cu NPs, BiVO$_4$/Bi NPs and BiVO$_4$/Bi-Cu composites, respectively. There's a negative shift in V$_{FB}$ potential for BiVO$_4$/Bi-Cu compared to other electrodes, indicates a decrease in bending band edge which leads to the facile transport of photogenerated carriers with low recombination thereby enhancing the PEC performance. Moreover, from the M-S plots, a smaller magnitude of the slope implies higher charge carrier concentration. As seen in the Fig. S5a, the BiVO$_4$/Bi-Cu photoanode revealed higher charge carrier density with lower slope, delivers the faster carrier transfer than the other samples, which is benefits from the enhanced PEC performance for hydrogen evolution reaction. Typically, the work function difference between the metal and the n-type semiconductor results in electrons transferred either from semiconductor to the metal nanoparticles or vice versa yielding a Schottky junction. According to the Mott-Schottky model, the Schottky barrier height (SBH) at the metal/n-type semiconductor interface can be related to the difference between the metal work function (W$_m$) and the electron affinity (χ_s) of the semiconductor. Typically, higher SBH indicates the photoexcited electron transfers from the metal nanoparticles to the semiconductor. Therefore, we can determine the electron transport direction by comparing the SBH changes of photoelectrodes. The SBH values were calculated in lnJ-V curve shown in Fig. S5b by using equation:

$$J_s = A^* T^2 \exp(-q\phi SBH /k_B T)$$

where ϕSBH is SBH at the zero bias, A* is the Richardson constant (112 A/cm^{2}K^2), k_B is the Boltzmann constant, and J_s is the zero-bias saturation current density. From intercepts and slopes of lnJ vs V plot, the calculated ϕSBH for BiVO$_4$, BiVO$_4$/Cu, BiVO$_4$/Bi and BiVO$_4$/Bi-Cu are 0.015, 0.019, 0.021 and 0.025 eV respectively. As a result, the SBH of Bi-Cu based electrode is shifted compared to that of individual plasmonic metals (Cu and Bi) which reflects the shift in the work function of Bi-Cu alloys compared to pure metals, which is attributed to the electron transport from Bi-Cu nanoparticles to the BiVO$_4$ conduction band, resulting in a relatively higher electron injection efficiency and current density than pure Bi or Cu decorated photoelectrodes. This enhancement in BiVO$_4$/Bi-Cu composite was attributed to the synergetic effect of Bi-Cu NPs, Bi has a broad absorption in the visible light and Cu is good for electron injection. Thus, the electrons were photoexcited when the visible light irradiated on the Bi nanoparticles and then fast transferred to the Cu nanoparticles. In this process, the electron concentration may become low for the charge recombination, but the high injection efficiency will make up this part of electron loss since the fast electron injection from the Cu nanoparticles into BiVO$_4$ conduct band. This result clearly indicates that the metal nanoparticles can be photoexcited as electron donors, and that the electrons transferred from metal nanoparticles to BiVO$_4$. The Schottky barrier analyses indicate that the photoexcited electrons transferred from metal nanoparticles to BiVO$_4$, resulting electron injection and light-harvesting efficiencies were improved for the Bi-Cu decorated photoelectrode. We investigate the role of the bi-metallic layers (Bi-Cu) to the energetics at the rectifying junction that subsequently improved the effective barrier height of the composite system as well as the degree of band bending near the semiconductor surface, thereby increasing the photovoltage, which responsible for the shift of onset potential for water splitting. Therefore, M-S plot and SBH analysis are good agreement with improved PEC performance for water splitting.

The mechanism of PEC performance by the ternary photoanode BiVO$_4$/Bi-Cu electrode is schematically presented in Fig. 5c. Here the simulated solar illumination of the electrode leads to the generation of electron/hole pairs in the conduction (CB)/valence bands (VB) of BiVO$_4$. The VB and CB positions of BiVO$_4$ are obtained from cyclic voltammetry (Fig. S6). The calculation of band positions in the energy level diagram are presented in (SI). The photogenerated holes in the VB of BiVO$_4$ react with water to produce oxygen. On the other hand, Bi-Cu ANPs assists the transport of photogenerated hot electrons through the high electrical conductivity of Cu NPs to CB of BiVO$_4$ via external circuit to the counter electrode (Pt) where protons are reduced to liberate hydrogen. In this hypothetical mechanism, the primary role of Bi-Cu ANPs is to expedite the transfer of electrons from the Bi-Cu to conduction band of BiVO$_4$ and further to back contact FTO.
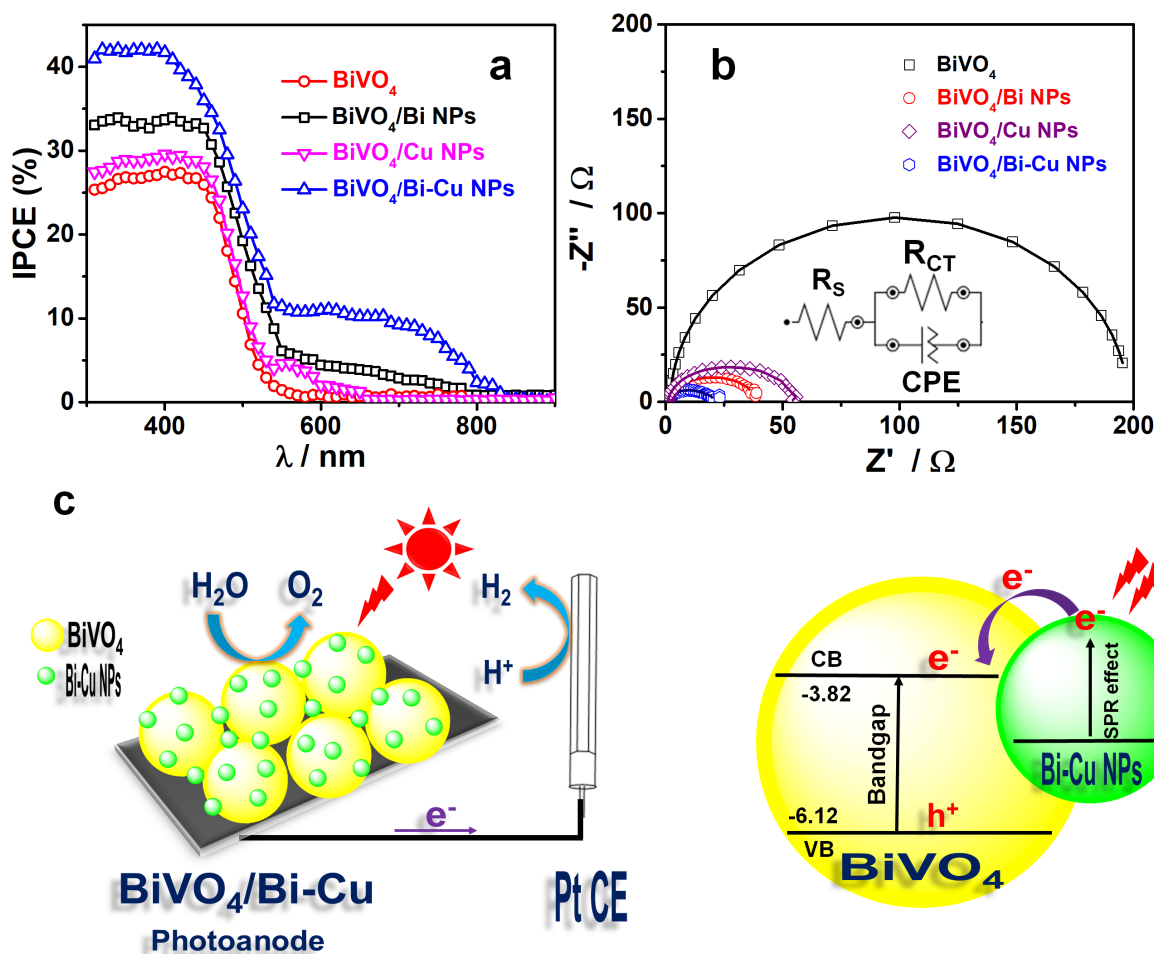
Fig. 5 (a) Wavelength-dependent IPCE plots, (b) electrochemical impedance plots (raw data (symbol) and fitted data (solid line)) of photoelectrodes and (c) scheme of a PEC cell constructed using the BiVO4/Bi-Cu photoanode, showing the charge transport and redox reactions under the light illumination.

Conclusions

To summarize, BiVO4/Bi-Cu photoanode was synthesized, characterized and tested for PEC water splitting. The proposed BiVO4/Bi-Cu photoanode exhibits high photocurrent density and long-term stability over 5 h under light illumination. Moreover, high H_2 evolution, low charge transfer resistance and high IPCE has been achieved for this composite. This enhancement in PEC water splitting is due to the synergetic effect of Bi-Cu ANPs displaying SPR features and high conductivity, thus Bi-Cu ANPs boost the visible light absorption and produce hot electrons near BiVO4 surface by LSPR excitation. These hot electrons are

transferred quickly resulting in low charge resistance that eventually enhances the photocurrent for PEC water splitting.

Acknowledgements

References

1. M. Grätzel, Photoelectrochemical cells, Nature 414 (2001) 338.

2. E.L. Miller, Photoelectrochemical water splitting, Energy Environ. Sci. 8 (2015) 2809-2810.

3. K. Sivula, R. Van De Krol, Semiconducting materials for photoelectrochemical energy conversion, Nat. Rev. Mater. 1 (2016) 15010.

4. O. Monfort, L.C. Pop, S. Sfaelou, T. Plecenik, T. Roch, V. Dracopoulos, E. Stathatos, G. Plesch, P. Lianos, Photoelectrocatalytic hydrogen production by water splitting using $BiVO_4$ photoanodes, Chem. Eng. J. 286 (2016) 91-97.

5. W. Luo, Z. Yang, Z. Li, J. Zhang, J. Liu, Z. Zhao, Z. Wang, S. Yan, T. Yu, Z. Zou, Solar hydrogen generation from seawater with a modified $BiVO_4$ photoanode, Energy Environ. Sci. 4 (2011) 4046-4051.

6. T.W. Kim, Y. Ping, G.A. Galli, K.S. Choi, Simultaneous enhancements in photon absorption and charge transport of bismuth vanadate photoanodes for solar water splitting, Nat. Commun. 6 (2015) 1-10.

7. V. Nair, C.L. Perkins, Q. Lin, M. Law, Textured nanoporous $Mo:BiVO_4$ photoanodes with high charge transport and charge transfer quantum efficiencies for oxygen evolution, Energy Environ. Sci. 9 (2016) 1412-1429.

8. A.J. Rettie, H.C. Lee, L.G. Marshall, J.F. Lin, C. Capan, J. Lindemuth, J.S. McCloy, J. Zhou, A.J. Bard, C.B. Mullins, Combined charge carrier transport and

photoelectrochemical characterization of $BiVO_4$ single crystals: intrinsic behavior of a complex metal oxide, J. Am. Chem. Soc. 135 (2013) 11389-11396.

9. S.S. Patil, M.G. Mali, M.A. Hassan, D.R. Patil, S.S. Kolekar, S.W. Ryu, One-Pot in situ hydrothermal growth of $BiVO_4$/Ag/rGO hybrid architectures for solar water splitting and environmental remediation, Sci. Rep. 7 (2017) 1-12.

10. M. Zhou, J. Bao, Y. Xu, J. Zhang, J. Xie, M. Guan, C. Wang, L. Wen, Y. Lei, Y. Xie, Photoelectrodes based upon Mo:$BiVO_4$ inverse opals for photoelectrochemical water splitting, ACS Nano 8 (2014) 7088-7098.

11. P. Subramanyam, T. Vinodkumar, D. Nepak, M. Deepa, C. Subrahmanyam, Mo-doped $BiVO_4$@ reduced graphene oxide composite as an efficient photoanode for photoelectrochemical water splitting, Catal. Today 325 (2019) 73-80.

12. O. Monfort, D. Raptis, L. Satrapinskyy, T. Roch, G. Plesch, P. Lianos, Production of hydrogen by water splitting in a photoelectrochemical cell using a $BiVO_4$/TiO_2 layered photoanode, Electrochim. Acta 251 (2017) 244-249.

13. S.Y. Jeong, H.M. Shin, Y.R. Jo, Y.J. Kim, S. Kim, W.J. Lee, G.J. Lee, J. Song, B.J. Moon, S. Seo, H. An, Plasmonic silver nanoparticle-impregnated nanocomposite $BiVO_4$ photoanode for plasmon-enhanced photocatalytic water splitting, J. Phys. Chem. C 122 (2018) 7088-7093.

14. S. Kim, Y. Yu, S.Y. Jeong, M.G. Lee, H.W. Jeong, Y.M. Kwon, J.M. Baik, H. Park, H.W. Jang, S. Lee, Plasmonic gold nanoparticle-decorated $BiVO_4$/ZnO nanowire heterostructure photoanodes for efficient water oxidation, Catal. Sci. Technol. 8 (2018) 3759-3766.

15. J.A. Seabold, K.S. Choi, Efficient and stable photo-oxidation of water by a bismuth vanadate photoanode coupled with an iron oxyhydroxide oxygen evolution catalyst, J. Am. Chem. Soc. 134 (2012) 2186-2192.

16. L. Zhang, C.Y. Lin, V.K. Valev, E. Reisner, U. Steiner, J.J. Baumberg, Plasmonic enhancement in $BiVO_4$ photonic crystals for efficient water splitting, Small 10 (2014) 3970-3978.

17. W. Yang, Y. Xiong, L. Zou, Z. Zou, D. Li, Q. Mi, Y. Wang, H. Yang, plasmonic Pd nanoparticle-and plasmonic pd nanorod-decorated $BiVO_4$ electrodes with enhanced photoelectrochemical water splitting efficiency across visible-NIR region, Nanoscale Res. Lett. 11 (2016) 1-8.

18. J. Wang, L. Tang, G. Zeng, Y. Liu, Y. Zhou, Y. Deng, J. Wang, B. Peng, Plasmonic Bi metal deposition and g-C_3N_4 coating on Bi_2WO_6 microspheres for efficient visible-light photocatalysis, ACS Sustain. Chem. Eng. 5 (2017) 1062-1072.

19. Q. Wang, J. He, Y. Shi, S. Zhang, T. Niu, H. She, Y. Bi, Designing non-noble/semiconductor $Bi/BiVO_4$ photoelectrode for the enhanced photoelectrochemical performance, Chem. Eng. J. 326 (2017) 411-418.

20. P. Subramanyam, T. Vinodkumar, M. Deepa, C. Subrahmanyam, Gold nanoparticle decorated bismuth sulfide nanorods for enhanced photoelectrochemical hydrogen production, J. Mater. Chem. C 7 (2019) 6398-6405.

21. J. Toudert, R. Serna, M. Jimenez de Castro, Exploring the optical potential of nano-bismuth: tunable surface plasmon resonances in the near ultraviolet-to-near infrared range, J. Phys. Chem. C 116 (2012) 20530-20539.

22. B.R. Wulan, S.S. Yi, S.J. Li, Y.X. Duan, J.M. Yan, X.B. Zhang, Q. Jiang, Non-noble-metal bismuth nanoparticle-decorated bismuth vanadate nanoarray photoanode for efficient water splitting, Mater. Chem. Front. 2 (2018) 1799-1804.

23. P. Subramanyam, T. Khan, G.N. Sinha, D. Suryakala, C. Subrahmanyam, Plasmonic Bi nanoparticle decorated $BiVO_4$/rGO as an efficient photoanode for photoelectrochemical water splitting, Inter. J. Hydrogen Energy 45 (2020) 7779-7787.

24. P. Zhang, T. Song, T. Wang, H. Zeng, In-situ synthesis of Cu nanoparticles hybridized with carbon quantum dots as a broad spectrum photocatalyst for improvement of photocatalytic H_2 evolution, Appl. Catal. B: Environ. 206 (2017) 328-335.

25. P. Zhang, T. Song, T. Wang, H. Zeng, Effectively extending visible light absorption with a broad spectrum sensitizer for improving the H_2 evolution of in-situ $Cu/g-C_3N_4$ nanocomponents, Inter. J. Hydrogen Energy 42 (2017) 14511-14521.

26. J. Li, Z. Liang, Y. Qin, L. Guo, N. Lei, Q. Song, Defective Bi_2WO_6-Supported Cu Nanoparticles as Efficient and Stable Photoelectrocatalytic for Water Splitting in Near-Neutral Media, Energy Technol. 6 (2018) 2247-2255.

27. P. Zhang, G. Zeng, T. Song, S. Huang, T. Wang, H. Zeng, Design of plasmonic CuCo bimetal as a nonsemiconductor photocatalyst for synchronized hydrogen evolution and storage, Appl. Catal. B: Environ. 242 (2019) 389-396.

28. P. Subramanyam, B. Meena, G.N. Sinha, M. Deepa, C. Subrahmanyam, Decoration of plasmonic Cu nanoparticles on WO_3/Bi_2S_3 QDs heterojunction for enhanced photoelectrochemical water splitting, Inter. J. Hydrogen Energy 45 (2020) 7706-7715.

29. P. Zhang, T. Song, T. Wang, H. Zeng, Plasmonic Cu nanoparticle on reduced graphene oxide nanosheet support: An efficient photocatalyst for improvement of near-infrared photocatalytic H_2 evolution, Appl. Catal. B: Environ. 225 (2018) 172-179.

30. S. Zhang, B. Peng, S. Yang, H. Wang, H. Yu, Y. Fang, F. Peng, Non-noble metal copper nanoparticles-decorated TiO_2 nanotube arrays with plasmon-enhanced photocatalytic hydrogen evolution under visible light, Inter. J. Hydrogen Energy 40 (2015) 303-310.

31. H. Li, X. Li, W. Dong, J. Xi, G. Du, Z. Ji, Cu nanoparticles hybridized with ZnO thin film for enhanced photoelectrochemical oxygen evolution, J. Alloys Compd. 768 (2018) 830-837.

32. K.K. Patra, C.S. Gopinath, Bimetallic and Plasmonic Ag-Au on TiO_2 for Solar Water Splitting: An Active Nanocomposite for Entire Visible-Light-Region Absorption, ChemCatChem 8 (2016) 3294-3311.

33. Y. Lu, J. Zhang, L. Ge, C. Han, P. Qiu, S. Fang, Synthesis of novel AuPd nanoparticles decorated one-dimensional ZnO nanorod arrays with enhanced photoelectrochemical water splitting activity, J. Colloid Interface Sci. 483 (2016) 146-153.

34. Y. Zhang, Y. Zhang, Y. Guo, L. Wu, Y. Liu, L. Song, Synthesis of AuPd nanoparticle-decorated graphene-coated ZnO nanorod arrays with enhanced photoelectrochemical performance and stability, RSC Adv. 9 (2019) 2666-2672.

35. K. Bhavani, G. Naresh, B. Srinivas, A. Venugopal, Plasmonic resonance nature of Ag-Cu/TiO_2 photocatalyst under solar and artificial light: Synthesis, characterization and evaluation of H_2O splitting activity, Appl. Catal. B: Environ. 199 (2016) 282-291.

36. Z. Jiao, Y. Zhang, S. Ouyang, H. Yu, G. Lu, J. Ye, Y. Bi, BiAg alloy nanospheres: a new photocatalyst for H_2 evolution from water splitting, ACS Appl. Mater. Interfaces 6 (2014) 19488-19493.

37. K. Bhunia, M. Chandra, S. Khilari, D. Pradhan, Bimetallic PtAu alloy nanoparticles-integrated g-C_3N_4 hybrid as an efficient photocatalyst for water-to-hydrogen conversion, ACS Appl. Mater. Interfaces 11 (2018) 478-488.

38. R.S. Moakhar, M. Jalali, A. Kushwaha, G.K.L. Goh, N. Riahi-Noori, A. Dolati, M. Ghorbani, AuPd bimetallic nanoparticle decorated TiO_2 rutile nanorod arrays for enhanced photoelectrochemical water splitting, J. Appl. Electrochem. 48 (2018) 995-1007.

39. E.S. Kim, H.J. Kang, G. Magesh, J.Y. Kim, J.W. Jang, J.S. Lee, Improved photoelectrochemical activity of $CaFe_2O_4$/$BiVO_4$ heterojunction photoanode by reduced surface recombination in solar water oxidation, ACS Appl. Mater. Interfaces 6 (2014) 17762-17769.

40. S. Ho-Kimura, S.J. Moniz, A.D. Handoko, J. Tang, Enhanced photoelectrochemical water splitting by nanostructured $BiVO_4$-TiO_2 composite electrodes, J. Mater. Chem. A 2 (2014) 3948-3953.

41. K. Sayama, A. Nomura, T. Arai, T. Sugita, R. Abe, M. Yanagida, T. Oi, Y. Iwasaki, Y. Abe, H. Sugihara, Photoelectrochemical decomposition of water into H_2 and O_2 on porous $BiVO_4$ thin-film electrodes under visible light and significant effect of Ag ion treatment, J. Phys. Chem. B 110 (2006) 11352-11360.

42. P. Subramanyam, B. Meena, D. Suryakala, M. Deepa, C. Subrahmanyam, Plasmonic nanometal decorated photoanodes for efficient photoelectrochemical water splitting, Catal. Today (2020).

43. T.W. Kim, K.S. Choi, Nanoporous $BiVO_4$ photoanodes with dual-layer oxygen evolution catalysts for solar water splitting, Science 343 (2014) 990-994.

44. X. Zhang, B. Zhang, K. Cao, J. Brillet, J. Chen, M. Wang, Y. Shen, A perovskite solar cell-TiO_2@$BiVO_4$ photoelectrochemical system for direct solar water splitting. J. Mater. Chem. A 3 (2015) 21630-21636.

45. M. Chiba, M.N. Thanh, Y. Hasegawa, Y. Obora, H. Kawasaki, T. Yonezawa, Synthesis of binary solid solution Cu-Pd nanoparticles by DMF reduction for enhanced photoluminescence properties. J. Mater. Chem. C 3 (2015) 514-520.

46. Q. Jia, K. Iwashina, A. Kudo, Facile fabrication of an efficient $BiVO_4$ thin film electrode for water splitting under visible light irradiation, Proc. Natl. Acad. Sci. 109 (2012) 11564-11569.

47. Q. Wang, T. Niu, L. Wang, C. Yan, J. Huang, J. He, H. She, B. Su, Y. Bi, FeF$_2$/BiVO$_4$ heterojuction photoelectrodes and evaluation of its photoelectrochemical performance for water splitting, Chem. Eng. J. 337 (2018) 506-514.

48. P. Subramanyam, B. Meena, G. Neeraja Sinha, D. Suryakala, C. Subrahmanyam, Facile Synthesis and Photoelectrochemical Performance of a Bi$_2$S$_3$@rGO Nanocomposite Photoanode for Efficient Water Splitting. Energy Fuels 35 (2021) 6315-6321.